

Electronic Supporting Information

Crystal structures and magnetic properties of chiral heterobimetallic chains based on the dicyanoruthenate building block

Jing Ru,^a Feng Gao,^a Min-Xia Yao,^b Tao Wu,^a and Jing-Lin Zuo^{*a}

^a *State Key Laboratory of Coordination Chemistry, School of Chemistry and Chemical Engineering, Nanjing National Laboratory of Microstructures, Nanjing University, Nanjing 210093, P. R. China*

^b *School of Science, Nanjing University of Technology, Nanjing 210009, P. R. China*

* To whom correspondence should be addressed. Email: zuojl@nju.edu.cn; Fax: +86-25-83314502.
Nanjing University.

Caption of Content

- 1. Table S1.** Selected bond lengths (\AA) and angles ($^\circ$) for complex **1**-(*SS*)
- 2. Table S2.** Selected bond lengths (\AA) and angles ($^\circ$) for complex **2**-(*SS*)
- 3. Figure S1.** CD spectra of **1**-(*RR*), **1**-(*SS*), (*R,R*)-H₂Salcy and (*S,S*)- H₂Salcy in KBr pellets
- 4. Figure S2.** CD spectra of **2**-(*RR*), **2**-(*SS*), (*R,R*)-H₂Salphen and (*S,S*)- H₂Salphen in KBr pellets
- 5. Figure S3.** Perspective drawing of the crystallographically structural of unit of **1**-(*SS*) showing the atom numbering. Hydrogen atoms are omitted for clarity.
- 6. Figure S4.** Perspective drawing of the crystallographically structural of unit of **2**-(*SS*) showing the atom numbering. Hydrogen atoms are omitted for clarity.
- 7. Figure S5.** Packing diagram of **1**-(*RR*) showing stacking interactions between the aromatic rings of the salcy ligand
- 8. Figure S6.** Plot of $1/\chi_M$ vs T for **1**-(*RR*). The red solid line is the fitting result by Curie-Weiss Law.
- 9. Figure S7.** Plot of $1/\chi_M$ vs T for **2**-(*RR*). The red solid line is the fitting result by Curie-Weiss Law.
- 10. Figure S8.** Top: Frequency dependence of the in-of-phase ac susceptibility (χ') of **2**-(*RR*) from 1.9 to 10 K at 0 Oe dc field. Bottom: Frequency dependence of the out-of-phase ac susceptibility (χ'') of **2**-(*RR*) from 1.9 to 10 K at a 0 Oe dc field.

Table S1 Selected bond lengths (Å) and angles (°) for complex **1**-(SS)

Ru(1)-N(1)	1.972(4)	Ru(1)-N(2)	1.990(3)
Ru(1)-O(2)	2.028(3)	Ru(1)-O(1)	2.040(3)
Ru(1)-C(17)	2.085(4)	Ru(1)-C(38)#1	2.077(4)
Mn(1)-O(3)	1.847(3)	Mn(1)-O(4)	1.875(4)
Mn(1)-N(5)	1.978(4)	Mn(1)-N(4)	1.989(4)
Mn(1)-N(3)	2.333(4)	Mn(1)-N(6)	2.346(4)
N(1)-Ru(1)-N(2)	83.10(15)	N(1)-Ru(1)-O(2)	90.16(14)
N(2)-Ru(1)-O(2)	171.09(15)	N(1)-Ru(1)-O(1)	173.18(14)
C(17)-N(3)-Mn(1)	157.9(4)	C(38)-N(6)-Mn(1)	155.6(3)
C(31)-N(4)-Mn(1)	124.8(4)	C(30)-N(4)-Mn(1)	112.3(3)
N(3)-C(17)-Ru(1)	171.4(4)	N(6)-C(38)-Ru(1)#2	175.5(5)
C(24)-N(5)-Mn(1)	123.0(4)	C(25)-N(5)-Mn(1)	113.2(3)
C(16)-O(1)-Ru(1)	124.6(3)	C(1)-O(2)-Ru(1)	122.8(3)
C(18)-O(3)-Mn(1)	125.5(3)	C(37)-O(4)-Mn(1)	128.0(3)

Symmetry transformations used to generate equivalent atoms: #1 $x+1, y, z$; #2 $x-1, y, z$

Table S2 Selected bond lengths (Å) and angles (°) for complex **2**-(SS)

C(90)-Ru(1)	2.034(7)	C(91)-Ru(1)	2.173(7)
Mn(1)-O(1)	2.032(5)	Mn(1)-N(1)	2.047(6)
Mn(1)-N(2)	2.049(6)	Mn(1)-O(2)	2.063(5)
Mn(1)-N(9)	2.297(7)	Mn(1)-N(10)	2.301(6)
Mn(3)-N(23)	2.352(6)	Mn(3)-N(24)	2.380(6)
Mn(3)-N(18)	2.029(6)	Mn(3)-N(17)	2.037(5)
N(3)-Ru(1)	2.072(6)	N(4)-Ru(1)	2.037(5)
N(7)-Ru(2)	2.023(6)	N(8)-Ru(2)	2.299(6)
O(7)-Ru(2)	2.055(5)	O(8)-Ru(2)	2.018(4)
O(3)-Ru(1)	2.068(4)	O(4)-Ru(1)	2.056(4)
N(9)-C(89)-Ru(2)#1	167.3(7)	N(10)-C(90)-Ru(1)	174.5(6)
N(11)-C(91)-Ru(1)	172.4(6)	N(12)-C(92)-Ru(2)	178.9(6)
N(1)-Mn(1)-N(10)	87.9(2)	N(2)-Mn(1)-N(10)	85.4(2)
O(2)-Mn(1)-N(10)	93.1(2)	N(9)-Mn(1)-N(10)	173.9(2)
C(7)-N(1)-Mn(1)	124.1(4)	C(8)-N(1)-Mn(1)	102.5(4)
C(10)-N(2)-Mn(1)	118.4(5)	C(9)-N(2)-Mn(1)	106.9(4)
C(183)-N(23)-Mn(3)	159.5(6)	C(184)-N(24)-Mn(3)	176.1(6)
C(38)-N(4)-Ru(1)	128.6(5)	C(37)-N(4)-Ru(1)	113.0(4)

Symmetry transformations used to generate equivalent atoms: #1 $x, y, z-1$; #2 $x, y, z+1$

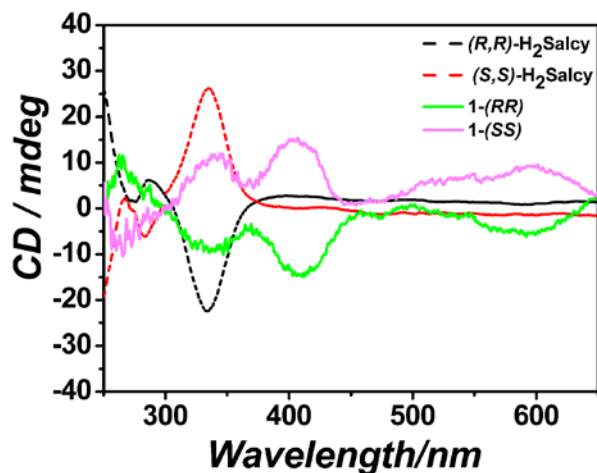


Figure S1. CD spectra of 1-(*RR*), 1-(*SS*), (*R,R*)-H₂Salcy and (*S,S*)- H₂Salcy in KBr pellets.

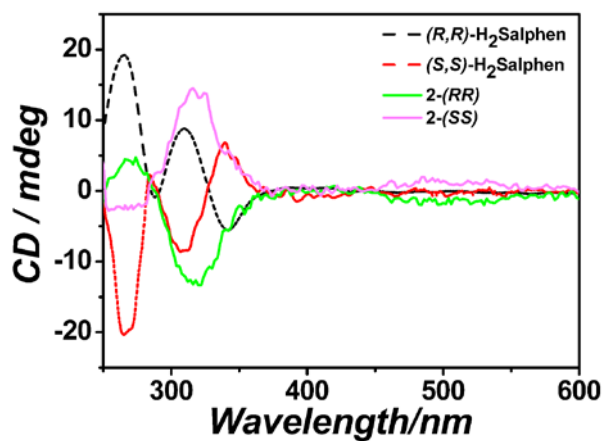


Figure S2. CD spectra of 2-(*RR*), 2-(*SS*), (*R,R*)-H₂Salphen and (*S,S*)- H₂Salphen in KBr pellets.

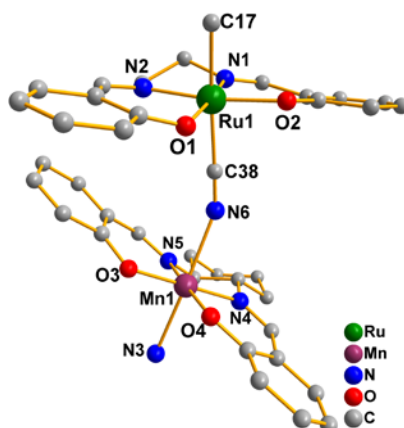


Figure S3. Perspective drawing of the crystallographically structural unit of 1-(*SS*) showing the atom numbering. Hydrogen atoms are omitted for clarity.

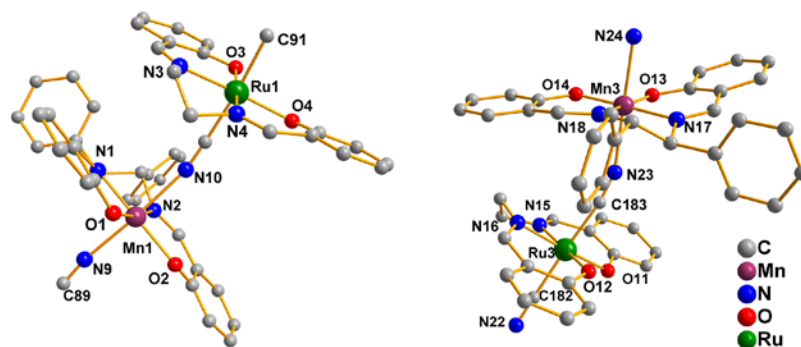


Figure S4. Perspective drawing of the crystallographically structural unit of **2-(SS)** showing the atom numbering. Hydrogen atoms are omitted for clarity.

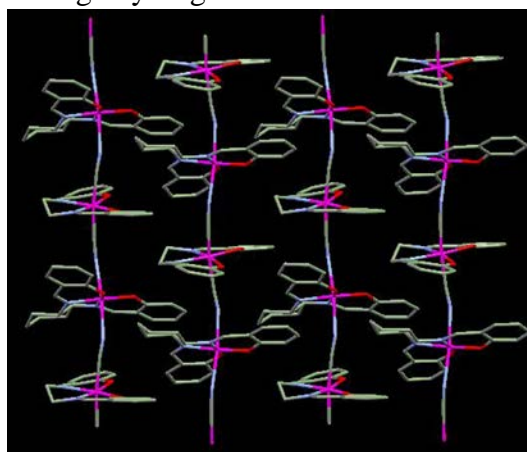


Figure S5. Packing diagram of **1-(RR)** showing stacking interactions between the aromatic rings of the salicy ligand.

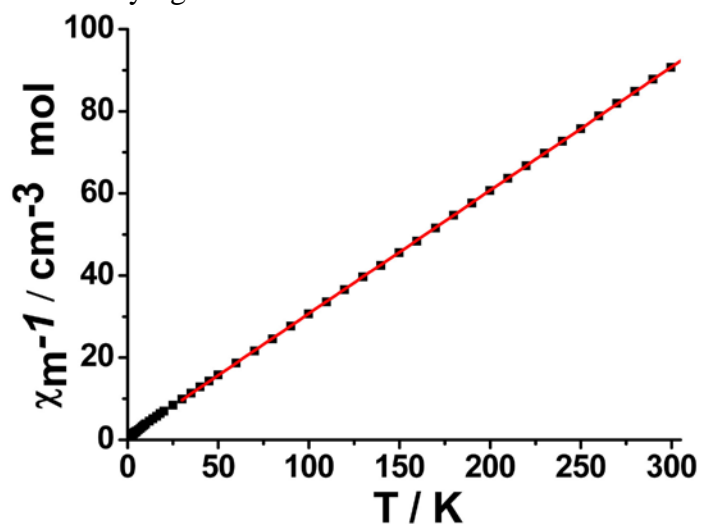


Figure S6. Plot of $1/\chi_M$ vs T for **1-(RR)**. The red solid line is the fitting result by Curie-Weiss Law.

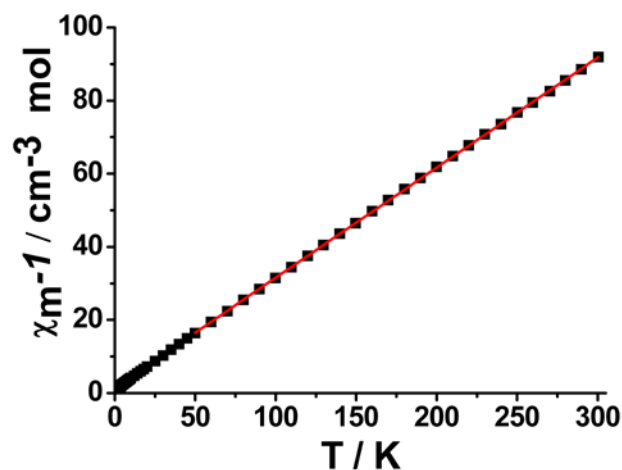


Figure S7. Plot of $1/\chi_M$ vs T for **2-(RR)**. The red solid line is the fitting result by Curie-Weiss Law.

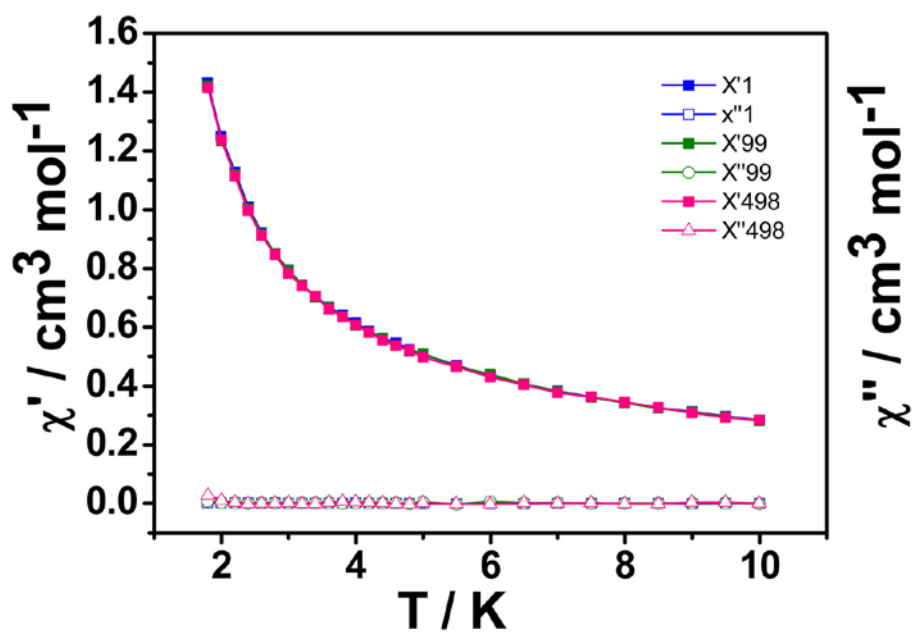


Figure S8. Top: Frequency dependence of the in-of-phase ac susceptibility (χ') of **2-(RR)** from 1.9 to 10 K at 0 Oe dc field. Bottom: Frequency dependence of the out-of-phase ac susceptibility (χ'') of **2-(RR)** from 1.9 to 10 K at a 0 Oe dc field.